

# CHALMERS



## Finding the Jeffrey Orbits

*Master's Thesis in Complex Adaptive Systems*

Staffan Ankardal

Department of Physics & Engineering Physics  
Non-linear Dynamics & Statistical Physics  
CHALMERS UNIVERSITY OF TECHNOLOGY  
Gothenburg, Sweden 2011  
Master's Thesis 2011:1

---

## Abstract

The Jeffrey orbits define the motion of axissymmetrical particles in shear flow and is thus important in the study of suspensions of particles. In these theses we verify the equations of motion experimentally using glass particles in a reversible flow in a PDMS microchannel and an optical tweezer. We also study the effects of asymmetry on the particles and study the transition from periodic to quasi-periodic orbits for different initial conditions and degrees of asymmetry. A good match with theoretical results are found, but there are some unexplained behaviours when the flow is reversed.

## Acknowledgements

I hereby wish to thank my girlfriend Callie Gibbons for supporting me through the work on this thesis and Alexander Laas for being a tireless and understanding co-worker. I want to thank my supervisors Bernhard Mehlig and Dag Hanstorp for helping with good suggestions. I want to thank all the contributors to the wealth of open source software which I have used to create everything from most of the software to more of the figures and of course this very report.

Staffan Ankardal, Göteborg Sweden INSERT PROPER DATE 3/11/13

# Contents

<b>1</b>	<b>Introduction</b>	<b>1</b>
1.1	Introduction . . . . .	1
1.1.1	Background . . . . .	1
<b>2</b>	<b>Theory</b>	<b>3</b>
2.1	Fluid Dynamics . . . . .	3
2.1.1	Navier Stokes . . . . .	3
2.1.2	Reynold's Number . . . . .	3
2.1.3	Stokes Drag and Stokes's law . . . . .	4
2.2	Euler Angles and our Coordinate System . . . . .	5
2.3	Jeffrey Orbits . . . . .	5
2.3.1	Winding Number . . . . .	8
<b>3</b>	<b>Method</b>	<b>9</b>
<b>I</b>	<b>Improvements of Experimental Setup</b>	<b>10</b>
3.1	Improvements . . . . .	11
3.1.1	Particles and Channel . . . . .	11
3.1.2	Automated Tracking . . . . .	14
3.2	Experimental Setup . . . . .	14
3.2.1	Density matching . . . . .	16
<b>II</b>	<b>Measurements and Analysis</b>	<b>17</b>
3.3	Data Analysis . . . . .	18
3.3.1	Particle identification . . . . .	18
3.3.2	Estimation of orientation . . . . .	19
3.3.3	Width compensation . . . . .	19
3.3.4	brushing . . . . .	20
<b>4</b>	<b>Results</b>	<b>21</b>

*CONTENTS*

---

<b>5 Discussion</b>	<b>22</b>
<b>A Raw data</b>	<b>23</b>

# 1

# Introduction

## 1.1 Introduction

The goal of this thesis is to study and better understand the dynamics of ellipsoidal particles in shear flow, and is a continuation of two previous masters theses [1, 2]. This is done by analysing micrometer length glass particles in a shear flow and comparing this to theoretical models. Before discussing either of these processes more in depth some background and basic theory is needed.

### 1.1.1 Background

The study of particle dynamics in flow began with Einstein's paper from 1905 [3] in which he showed that the viscosity of suspended particles would increase the viscosity of the fluid and by how much. Jeffrey in his 1922 paper [4] extended these results to ellipsoidal axis-symmetrical particles as well as derived equations for the orientational dynamics of the particles. For systems where inertial effects could be discarded the motion was found to be periodic and depending only on the initial condition of the particle.

Developments on triaxial particles, started with Gierszewski & Chaffey (1978)[5] and was continued by Hinch & Leal (1979)[6] and more recently by Yarin et al in 1993[7]. The dynamics found for axis-symmetric particles by Jeffrey were periodic, but it was shown by Hinch & Leal that some orbits would be doubly periodic, in other words following two separate independent periods. Yarin then was able to use numerical simulations to generate a surface of section [8] for some asymmetric relations between the two minor axes showing that not only was there double periodic or quasi periodic orbits but for sufficiently large asymmetries in axes there would be chaotic orbits. Several other surfaces of were also produced by Johansson (2012)[1] using the same method as Yarin with higher resolution thanks to improvements in computing power. It was there shown that only very small asymmetries on the order of 1% will lead to quasi-periodic motion for some initial conditions.

Experimental studies of these theoretical results were first done by Goldsmith and Mason in 1962[9] who confirmed that the rotation rate matched well with that predicted from Jeffrey orbits but he did not study the actual orbits. Since then most experimental research, such as by Harlen

## *1.1. INTRODUCTION*

---

and Koch[10] has been focused on diluted suspensions of particles and the increased viscocity and other properties this causes. Only tangential efforts such as by Tolga[11] were concerned with the Jeffrey orbits. A good summary of both theoretical and experimental results was written by Petrie in 1999 [12].

The first dedicated experimental work to try to measure the actual Jeffrey orbits and study the orientational dynamics was done by Einarsson et al [13] in 2011. Although there was some promising results, the vast majority of particles were asymmetric to the point of chaotic or highly quasi-periodic. Moreover the width and length of particles both varied great and could not be measured with good accuracy, meaning that the aspect ratio could not accurately be determined.

# 2

## Theory

In order to better understand the results and discussions in this thesis some rather basic results in fluid dynamics, image analysis and other fields need to be understood by the reader.

1) It is however not the focus of this thesis and as such I will try to be as brief as possible, and an experienced reader can safely skip to the next chapter.

OR

2) As the focus of this thesis is experimental I will not go into great detail, but try to briefly motivate and quickly summarize results, and refer the inquisitive reader to more thorough sources. As no recent developments are discussed, readers comfortable in these fields can skip this chapter without any loss in understanding.

### 2.1 Fluid Dynamics

In order to understand the motivations, limitations and behaviour of the experiment we need to know about a few key concepts in fluid dynamics.

#### 2.1.1 Navier Stokes

#### 2.1.2 Reynold's Number

The Reynolds number ( $Re$ ) is a dimensionless number describing the ratio of inertial forces to viscous forces in a flow. This is not a very strict definition, but suffices to explain that the Reynolds number can be used to characterize the so called flow regime of a system.

The two major flow regimes are Laminar flow, where viscous forces dominate over inertial forces, and the turbulent regime where inertial forces dominate. The area where neither is significantly larger is referred to as transitional flow, which may show either chaotic or laminar behaviour.

A rough characterization of laminar and chaotic flow can be seen in figure 2.1

The Reynolds number ( $Re$ ) is defined as [14]

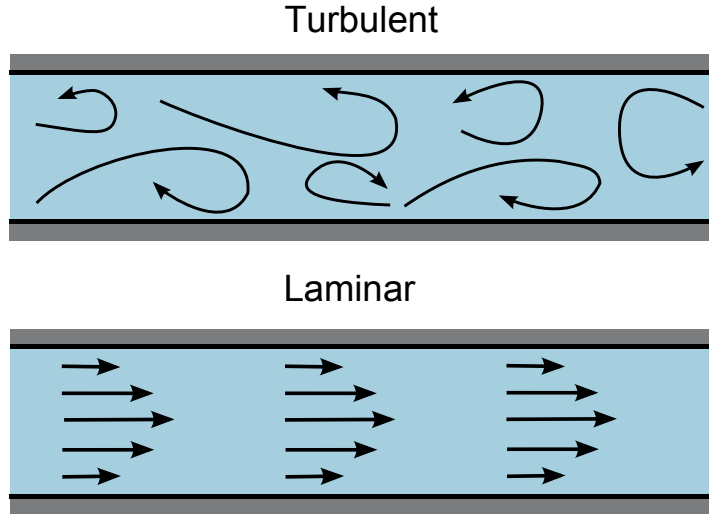


**Figure 2.1:** This shows the principal difference between laminar and turbulent flow

$$Re = \frac{UL\rho}{\mu} \quad (2.1)$$

where  $U$  is the characteristic velocity,  $L$  is the characteristic length,  $\rho$  is the density and  $\mu$  is the dynamic viscosity.

As the Reynolds number is a ratio, a flow is predicted to be laminar if  $Re \ll 1$  which is the primary concern in this thesis.

### 2.1.3 Stokes Drag and Stokes's law

The drag force  $F_D$  exerted by a fluid on a spherical particle for  $Re \ll 1$  is found using the so called Stokes's law [15]

$$F_D = 6\pi\mu Rv \quad (2.2)$$

where  $v$  is the velocity of the sphere relative to the fluid,  $\mu$  is the dynamic viscosity and  $R$  is the radius of the sphere. To find the terminal velocity of the sphere we equate this with the gravitational force  $F_G$  acting on the sphere

$$F_G = \Delta\rho g \cdot \frac{4\pi R^3}{3} \quad (2.3)$$

where  $\Delta\rho$  is the difference in density and  $g$  is the specific gravity we find that the terminal velocity of a sinking (or floating) sphere is

$$v_s = \frac{2}{9} \frac{\Delta\rho}{\mu} g R^2 \quad (2.4)$$

## 2.2 Euler Angles and our Coordinate System

When describing rotating particles it is common to use the so called Euler Angles. A formal definition can be found at MathWorld [16] but for the purposes of this thesis we will describe it as a transformation from a coordinate system  $\{x,y,z\}$  to  $\{x',y',z'\}$  in three steps

- Rotate the x-y plane  $\phi$  about the z-axis.
- Denote the shifted x axis T and rotate the z-y' plane  $\theta$  around this axis
- Rotate  $\psi$  around the z' axis to obtain the final coordinate system

This is illustrated in figure 2.2 where each prim marks one more step of rotation to the coordinate system. To make it clear how this relates to the experiment figure 2.3 shows the euler angle rotations for a triaxial particle shown from a point of view similar to the of the experiment where the X-Z plane is the primary plane.

## 2.3 Jeffrey Orbits

The equations of motion for a triaxial ellipsoid particle was first found by Jeffrey [4] but the first dimensionless equation for the Euler Angles was found by Yarin et al. [7] to be

$$\frac{d\theta}{dt} = (g_2 \sin \psi + g_3 \cos \psi) \sin \theta \quad (2.5a)$$

$$\frac{d\phi}{dt} = \frac{1}{2} + g_3 \sin \psi - g_2 \cos \psi \quad (2.5b)$$

$$\frac{d\psi}{dt} = g_1 + (g_2 \cos \psi - g_3 \sin \psi) \cos \theta \quad (2.5c)$$

$$(2.5d)$$

where the functions  $g_i$  are defined as

$$g_1 = \frac{a_y^2 - a_z^2}{2(a_y^2 + a_z^2)} \left( -\frac{1}{2}(\cos^2 \theta + 1) \sin 2\phi \sin 2\psi + \cos \theta \cos 2\phi \cos 2\psi \right), \quad (2.6a)$$

$$g_2 = \frac{a_z^2 - a_x^2}{2(a_x^2 + a_z^2)} \left( -\cos \theta \sin 2\phi \sin \psi + \cos 2\phi \cos \psi \right), \quad (2.6b)$$

$$g_3 = \frac{a_x^2 - a_y^2}{2(a_x^2 + a_y^2)} \left( \cos \theta \sin 2\phi \cos \psi + \cos 2\phi \sin \psi \right) \quad (2.6c)$$

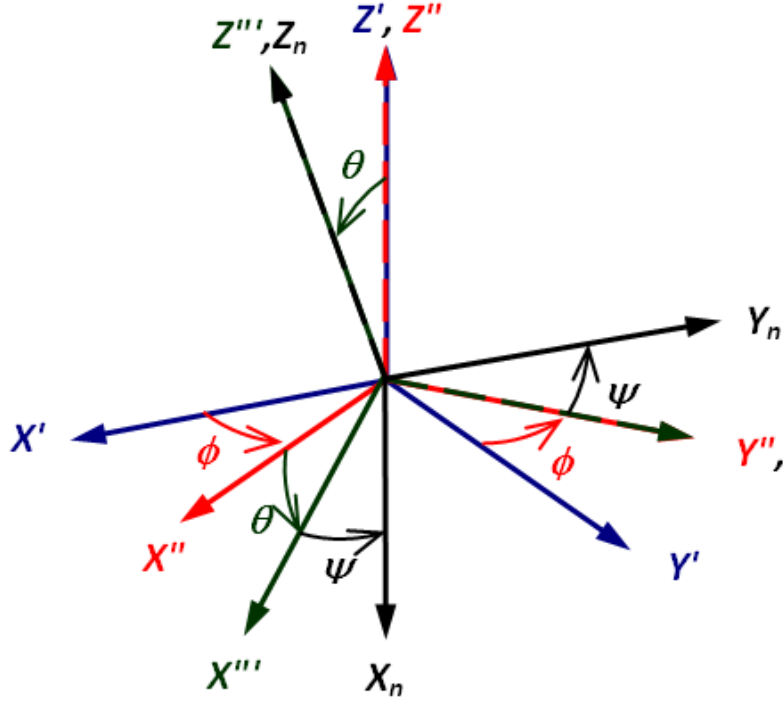


**Figure 2.2:** The Euler angles illustrated using a series of coordinate rotations. This is the normal way of illustrating the Euler angles as it is how they are defined.

where the angles are defined as can be seen in figure 2.2. It should be noted that the Jeffrey orbits sometimes refer simply to solution for the symmetric case (as found by Jeffrey) but this leaves the asymmetric orbits unnamed, so in this thesis Jeffrey Orbits refer to the solutions for both symmetric and asymmetric particles.

The orbits for different initial conditions can be plotted in a Poincaré map [17] for  $\phi = 0$ . A few such maps can be seen in figure ???. A simplified explanation of the Poincaré map is that a particle starting on some point on a line in the map will follow along that line the next time it intersects with the section, in our case when the particle has  $\phi = 0$ .

For a particle with a small asymmetry there are essentially three classes of orbits.

1. Periodic. For larger  $|\theta|$  there is little variation and the particle is largely periodic with fluctuations too small to measure.
2. Quasi-periodic bent: For intermediate  $|\theta|$  the amplitude of  $\cos(\theta)$  changes noticeably but does not change sign.
3. Quasi-periodic circular: For small  $|\theta|$  the amplitude of  $\cos(\theta)$  will change noticeably and change sign from positive to negative.

These three different types of orbits are illustrated in 2.4 and also shows .

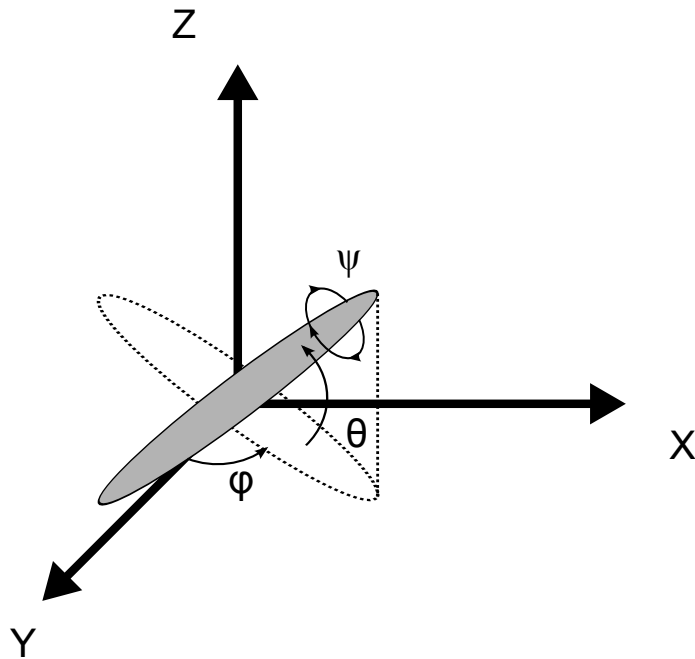


**Figure 2.3:** The Euler angles illustrated using an ellipsoid. This alternate visualization shows the angles with a point of view similar to that of the camera in the experiment. Note although  $\psi$  has an impact on the particle dynamics, as the particle is nearly axis-symmetric we can not observe it

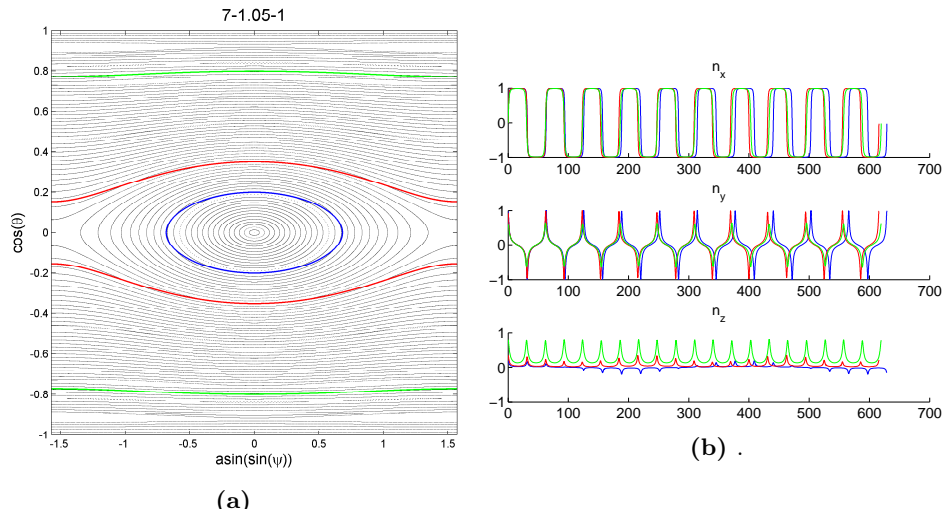


**Figure 2.4:** WRITE PARAMETERS HERE THEY ARE LAMBDA 7 EPSILON 5.

### 2.3.1 Winding Number

The quasi-periodic orbits are also referred to as double-periodic. This is referring to the fact that the variations that are seen in figure 2.4b are periodic as well. The ratio between the two periods is referred to as the winding number  $\omega$ , or simply

$$\omega = \frac{\theta_1}{\theta_2}. \quad (2.7)$$

This can also be thought of as the number of steps travelled on the poincare map before coming back to where it started, divided by the number of laps it takes. This number is the same for any point along a given orbit on the poincare map but varies greatly for different orbits as well as for different asymmetries. The winding numbers for orbits a slice along  $\psi = 0$  for  $\epsilon = \{0.01, 0.05, 0.10\}$  can be seen in figure 2.5

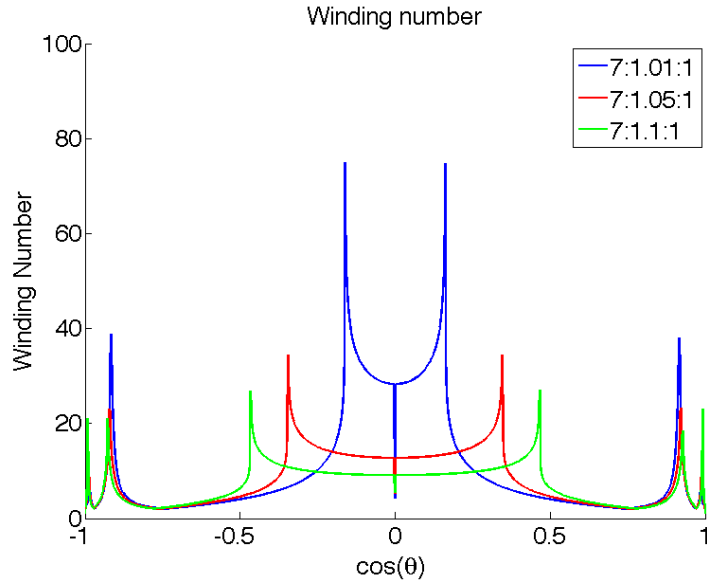


**Figure 2.5:** The winding number as a function of  $\cos(\theta)$  for three different asymmetries. The sharp edge that occurs centered around zero is when the circular orbits break into bent orbits as mentioned previously. We see that a lower asymmetry leads to a sharper difference between the circular and the bent orbits.

# 3

## Method

# **Part I**

## **Improvements of Experimental Setup**

### 3.1. IMPROVEMENTS

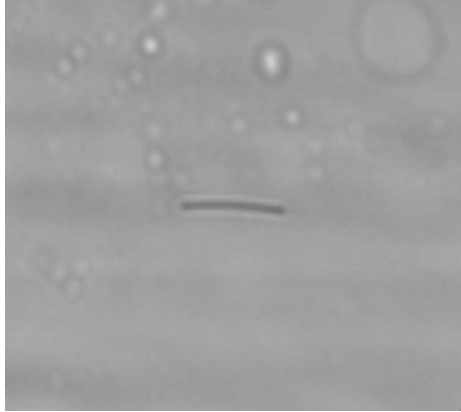
---

As previously mentioned this thesis is a continuation of work done by Mehlig, Einarsson and Mishra et al [1, 13, 18]. Their results were promising but there were a number of key limitations and problem that we want to solve to improve the results and the ease of getting results. Roughly they are

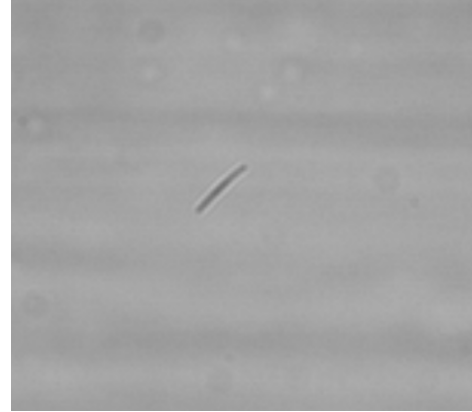
1. The particles
  - Very few particles are symmetric, most are visibly bent or uneven, see figure 3.1
  - Few particles have a low enough aspect to be useful.
  - Have greatly varying and difficult to measure width meaning the aspect ratio cannot be estimated well
  - Cannot be trapped with an optical tweezer due to low transmittance
2. The PDMS in the channel is very jagged which causes a great deal of noise unless the focus is in a very narrow band
3. Manual tracking of particles is time consuming and mentally draining.
4. Bubbles are difficult to avoid when setting up the experiment

## 3.1 Improvements

### 3.1.1 Particles and Channel



(a) Particle 13 from July 2012



(b) Particle 22 from July 2012

**Figure 3.1:** Two fairly typical particles from the previous setup. Note that these are still selected from the total pool of particles for being relatively symmetric and yet are noticeably bent.

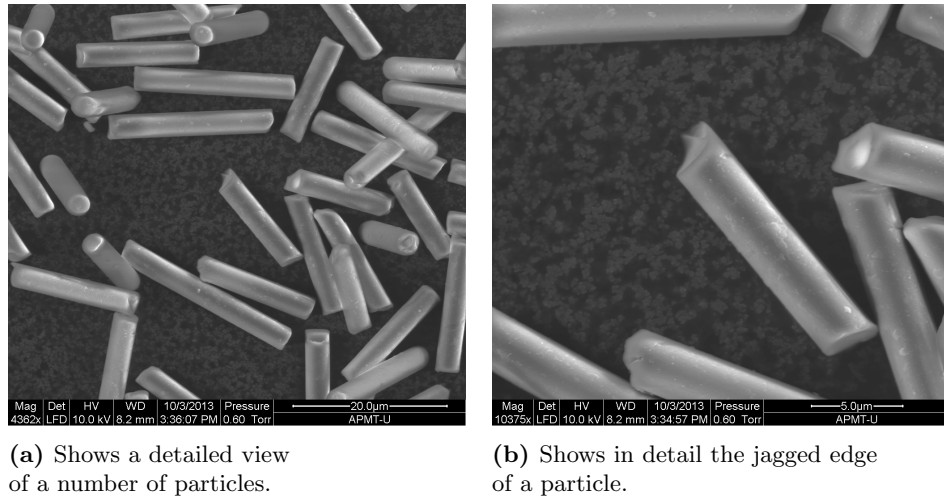
To solve the problems with the particles we replaced them with glass particles from Nippon Glass, Japan [19]. The particles are made from LCD spacing rods that are , which means they are essentially broken cylinders with very consistent width but quite varying length. Two different batches of particles have been used, one with  $3\mu m$  diameter and one batch with  $5\mu m$  diameter. All

### 3.1. IMPROVEMENTS

---

the particles presented in the results section are from the  $3\mu\text{m}$  batch. To verify that the particle were indeed as symmetric and with as even width as we suspected images were taken with an ESEM (Environmental Scanning Electron Microscope) and can be seen in figure 3.2. We see that the particles are uniformly smooth along the edges but have varyingly jagged edges causing different degrees of asymmetry.

In particular figure 3.3b shows a top down view of a particle clearly showing a very circular shape with no discernible asymmetry.



(a) Shows a detailed view  
of a number of particles.

(b) Shows in detail the jagged edge  
of a particle.

**Figure 3.2:** Pictures of the glass particles that particles

### 3.1. IMPROVEMENTS

---

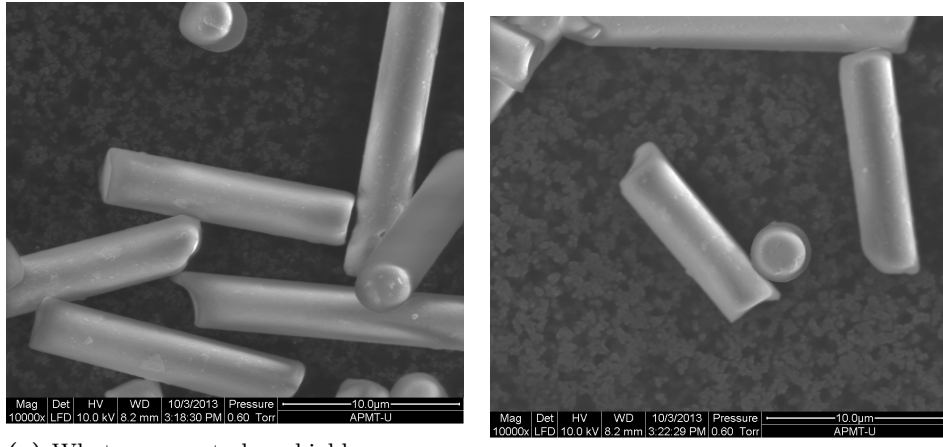


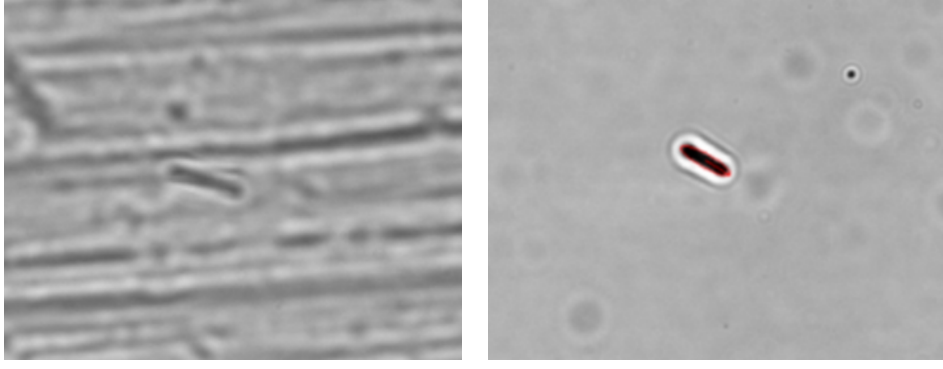
**Figure 3.3:** Pictures highlighting the roundness of the particles as well as the apparent symmetry of some particles. It should be noted that although there are no apparent rough edges there was no way to rotate a sample so there might very well be asymmetries on the side of the particle that we cannot see.

While these particles seemingly satisfy the symmetry conditions they are made glass with a density of approximately  $2.57 \text{ g/cm}^3$  at  $20^\circ\text{C}$  which is significantly higher than that of water with a density of  $1 \text{ g/cm}^3$  at  $20^\circ\text{C}$  and glycerol with a density of  $1.5 \text{ g/cm}^3$ . Thus to correct for the density and limit sinking or floating the water soluble Sodium metatungstate which at  $20^\circ\text{C}$  has maximum density of  $2.94 \text{ g/cm}^3$ . To increase the viscosity of the liquid around 8% glycerol is added, resulting in a measured dynamic viscosity of  $24 \cdot 10^{-3} \text{ Pa s}$

A problem in finding and tracking a particle was that the surface of the PDMS was very uneven and one could see sharp ridges along the length of the channel like in figure 3.4a unless the focus was in a relatively narrow depth of the channel.

### 3.2. EXPERIMENTAL SETUP

---



(a) An unusual severe case of the PDMS edges creating noise. (b) After being polished there is no trace of such ridges.

**Figure 3.4:** Pictures highlighting the roundness of the particles as well as the apparent symmetry of some particles. It should be noted that although there are no apparent rough edges there was no way to rotate a sample so there might very well be asymmetries on the side of the particle that we cannot see.

This was fixed by polishing the copper mold in which the PDMS channels are formed with a silicate abrasive (Autosol) and emery cloth. This reduces all visible scratches from the mold and thus from the PDMS and the result can be seen in figure 3.4b.

#### 3.1.2 Automated Tracking

### 3.2 Experimental Setup

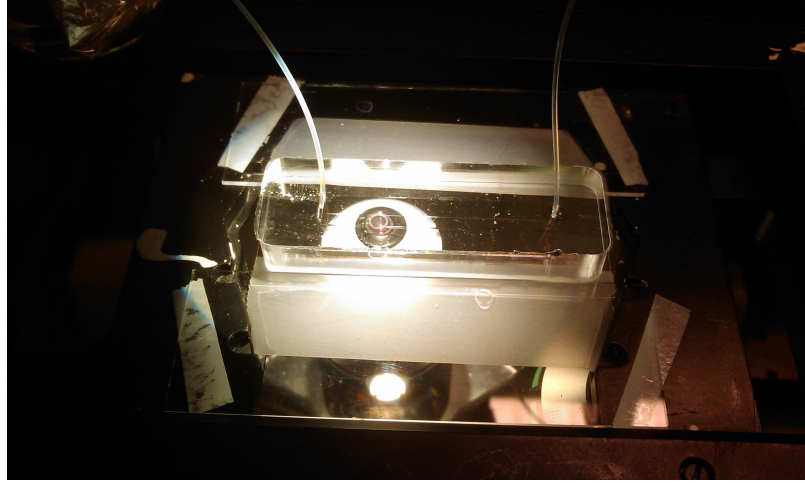
As the goal is to attempt to verify the Jeffrey equations in eq 2.5 we need an experimental setup with particles and flow system that satisfy the conditions that the Jeffrey equations apply under. This means our particles have to be buoyant, triaxially symmetric and small enough that inertial effects are negligible. The flow has to be a linear creeping flow, in other words have a Reynolds number satisfying  $Re \ll 1$  and have a high unidirectional shear that allows one to detect the orbits in a relatively short distance.

The particles used in previous measurements were made from epoxy mixed in a vortex[13] which made them buoyant and small enough to ignore inertial effects, but they were not symmetrical enough to produce reliable periodic Jeffrey orbits. Thus two sets of glass particles from Nippon Glass, Japan[19], have been used. They are cylindrical with a consistent width of  $3\text{ }\mu\text{m}$  and  $5\text{ }\mu\text{m}$  and varying length. Images taken with a STEM microscope can be seen in figure 3.2.

While these particles seemingly satisfy the symmetry conditions they are made glass with a density of approximately  $2.57\text{ g/cm}^3$  at  $20\text{ }^\circ\text{C}$  which is significantly higher than that of water with a density of  $1\text{ g/cm}^3$  at  $20\text{ }^\circ\text{C}$  and glycerol with a density of  $1.5\text{ g/cm}^3$ . Thus to correct for the density and limit sinking or floating the water soluble Sodium metatungstate which at  $20\text{ }^\circ\text{C}$  has maximum density of  $2.94\text{ g/cm}^3$ . To increase the viscosity of the liquid around 8% glycerol is added, resulting in a measured dynamic viscosity of  $24 \cdot 10^{-3}\text{ Pa s}$

### 3.2. EXPERIMENTAL SETUP

---



This liquid with suspended particles is flowed through a channel of Polydimethylsiloxane (PDMS) 4 cm long, 2.5 mm wide and either 200  $\mu\text{m}$  and 500  $\mu\text{m}$ . The flow profile of such a channel was calculated by Anton Johansson in his thesis[1] and can be seen in figure 3.5. The flow rate varies between 2 and 20  $\mu\text{l}/\text{m}$  or in SI units  $3.33 \cdot 10^{-10} \text{ m}^3/\text{s}$  which with a cross section of at least  $5 \cdot 10^{-7} \text{ m}^2$  means a maximum flow speed of 6.66  $\text{mm}/\text{s}$ .

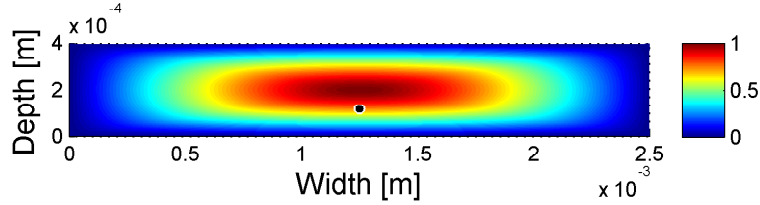


**Figure 3.5**

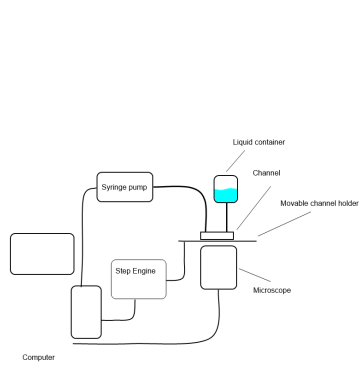
To confirm that the flow is a creeping flow we can calculate the maximum Reynolds number using eq 2.1 and our maximum flow speed

$$Re = \frac{UL\rho}{\mu} \leq \frac{6.66 \cdot 10^{-3} \cdot 2.5 \cdot 10^{-3} \cdot 2.5}{24 \cdot 10^{-3}} \approx 1.6 \cdot 10^{-3} \ll 1 \quad (3.1)$$

This should satisfy the conditions of the Jeffrey equations. To track the particles the channel is put in a moveable stage on a confocal microscope. The entire setup can be seen in figure 3.6

### 3.2. EXPERIMENTAL SETUP

---



(a) Sketch of the set up



(b) Overview of the set up

**Figure 3.6**

#### 3.2.1 Density matching

$$\rho_a = \frac{m_a}{V_a} = \frac{V_b \rho_b + V_{mix} \rho_{mix}}{V_b + V_{mix}} \quad (3.2)$$

So if we want to find  $V_{mix}$  we get

$$V_{mix} = \frac{V_b(\rho_b - \rho_a)}{\rho_a - \rho_{mix}} \quad (3.3)$$

## **Part II**

# **Measurements and Analysis**

### 3.3 Data Analysis

Once a movie had been recorded we want to estimate the dynamics of the particle. This is done in several steps.

#### 3.3.1 Particle identification

The first step is to reduce the static noise from the movie caused by dirt, scratches and other defects in the microscope and on the camera lens as can be seen in figure 3.7aAs the noise is static and everything else changes this is a simple matter of computing an average frame

$$\bar{F} = \frac{\sum_{n=1}^N F}{den} \quad (3.4)$$

an example of such an average frame can be seen in figure 3.7b. This is then removed from the camera frame and the result can be seen in figure 3.7c. After this we apply a smoothing function and Canny edge detection [? ] and then fill the resulting edge. The resulting pixels are then fit to an ellipse as described in [1? ]. The filled contour and the fit ellipse can be seen in figure 3.7d.

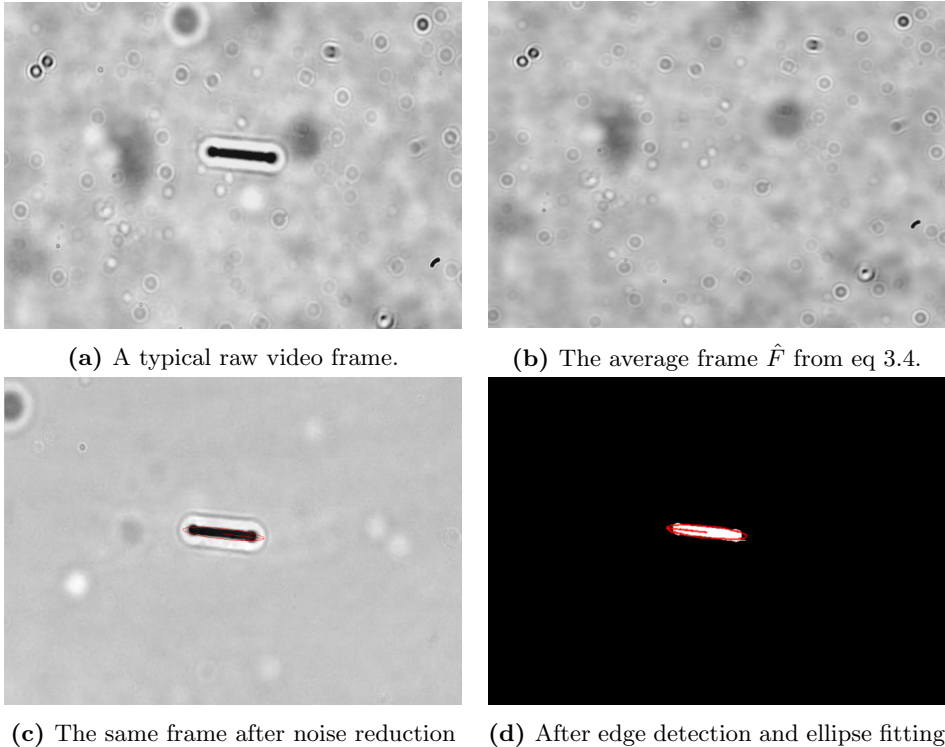


**Figure 3.7:** These pictures show a simplified version of the image analysis from raw image to estimated particle position

### 3.3.2 Estimation of orientation

The ellipsoid we get is then our best approximation of the projection of the actual particle. In order to normalize  $\mathbf{n}$  we need to know the length of the particle. However as it was shown by Leal that the particle will always spend a majority of its time aligned with the flow, ie aligned with the camera which means that by simply calculating the length  $L$  every frame and finding the mode of the distribution we will find a good estimate of  $L$ .

So given an ellipsoid with length  $l_e$ , width  $d_e$  and angle  $\phi_p$  we find

$$p_x = l_e * \sin(\phi_p) \quad (3.5)$$

$$p_z = l_e * \cos(\psi_p) \quad (3.6)$$

with x and z projection  $p_x$  and  $p_z$  we can get  $n_x$  and  $n_z$  as well as  $n_y$  via

$$n_x = \frac{p_x}{L} \quad (3.7a)$$

$$n_z = \frac{p_z}{L} \quad (3.7b)$$

$$n_y = \sqrt{1 - n_x^2 - n_z^2} \quad (3.7c)$$

### 3.3.3 Width compensation

Up until this point we have assumed that the particle is a *thin* rod so that the projection  $\mathbf{p}$  onto the x and z-axes give us an accurate estimate of  $\mathbf{n}$ . However when we are projecting 'thick' particle with length  $L$  and width  $D$  we get  $\mathbf{n}'$ . At  $\phi = 0$  this is

$$\mathbf{n}' = n'_z = n_z \cos(\theta) + D \sin(\theta) \quad (3.8)$$

which is illustrated in figure 3.8.

In order to compensate for this error we modify our projection equation 3.5 to

$$p_x = (l_e - w_e) * \sin(\phi_p) \quad (3.9)$$

$$p_z = (l_e - w_e) * \cos(\psi_p) \quad (3.10)$$

This will reduce the particles estimated length by  $w_e$

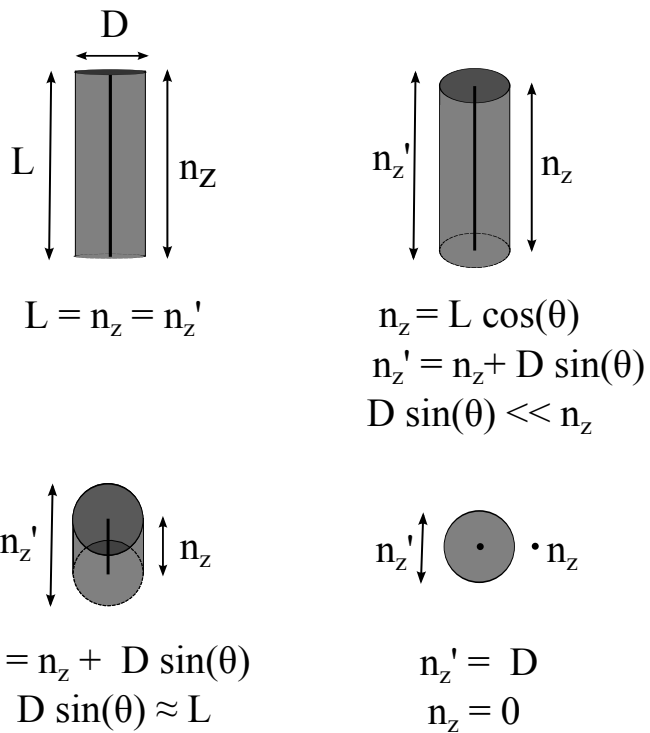


Figure 3.8

### 3.3.4 brushing

# 4

## Results

The measurements in this section was done together with Alexander Laas.

# 5

## Discussion

A

Raw data

# Bibliography

- [1] J. A., Analysis of empirical data on the tumbling of microrods in a shear flow, Master's thesis, Chalmers University of Technology.
- [2] E. J., Low reynolds number particle dynamics, Master's thesis, Chalmers University of Technology.
- [3] A. Einstein, A new determination of molecular dimensions, Annalen der Physik.
- [4] G. B. Jeffrey, The motion of ellipsoidal particles immersed in a viscous fluid, Proceedings of the Royal Society A 102.
- [5] P. J. Gierszewski, C. E. Chaffey, Rotation of an isolated triaxial ellipsoid suspended in slow viscous flow, Canadian Journal of Physics 56 (1) (1978) 6–11.
- [6] L. G. L. E. J. Hinch, Rotation of small non-axissymmetrical particles in a simple shear flow, J. Fluid Mech 92 (1979) 591–608.
- [7] I. V. R. A. L. Yarin, O. Gottlieb, Chaotic rotation of triaxial ellipsoids in simple shear flow, J. Fluid Mech vol 340 (1997) 83–100.
- [8] F. C. van den Bosch, lecture 1: Surfaces of section, Online material for course.
- [9] S. G. M. H. L. Goldsmith, The flow of suspensions through tubes i. single spheres, rods, and discs, Journal of colloid science (17).
- [10] D. K. O.G. Harlen, Orientational drift of a fibre suspended in a dilute polymer solution during oscillatory shear flow, J. Non-Newtonian Fluid Mech. 73 (1997) 81–93.
- [11] T. Kaya, H. Koser, Characterization of hydrodynamic surface interactions of escherichia coli cell bodies in shear flow, Phys. Rev. Lett. 103 (2009) 138103.
- [12] C. J. S. Petrie, The rheology of fiber suspensions, J. of non-newtonian fluid mechanics 87.
- [13] J. E. et al, Periodic and aperiodic tumbling of microrods advected in a microchannel flow, Acta Mechanica (2013) 1–9.

## BIBLIOGRAPHY

---

- [14] T. Pedley, Introduction to Fluid Dynamics, Department of Applied Mathematics and Theoretical Physics, University of Cambridge, Silver St., Cambridge CB3 9EW, U.K., 1997.
- [15] G. K. Batchelor, An Introduction to Fluid Dynamics, Cambridge University Press, 1967, page 212 is definition of Reynolds Number, page 233 is Stokes Law.
- [16] W. E. W, Euler angles, from MathWorld—A Wolfram Web Resource. (2013).  
URL <http://mathworld.wolfram.com/EulerAngles.html>
- [17] J. Munkhammar, Poincare map (2013).  
URL [mathworld.wolfram.com/PoincareMap.html](http://mathworld.wolfram.com/PoincareMap.html)
- [18] J. E. e. a. Y. N. Mishra, A microfluidic device for studies of the orientational dynamics of microrods, Proc. SPIE 8251 2825109.
- [19] N. E. G. Co, Gap spacers for lcds: Microrods, [www.neg.co.jp/epd/elm/e\\_prd/other/others\\_01.pdf](http://www.neg.co.jp/epd/elm/e_prd/other/others_01.pdf).